Compel

A magnetic network approach to the transient analysis of synchronous machines

M. Andriollo
Department of Electrical Engineering – Politecnico di Milano, Milano, Italy
T. Bertoncelli
Department of Electrical Engineering – Politecnico di Milano, Milano, Italy
A. Di Gerlando
Department of Electrical Engineering – Politecnico di Milano, Milano, Italy

COMPEL, Vol. 22 No. 4, 2003,
 ISSN 0332-1649

A magnetic network approach to the transient analysis of synchronous machines

M. Andriollo, T. Bertoncelli and A. Di Gerlando
Department of Electrical Engineering – Politecnico di Milano, Milano, Italy

Keywords *Magnetic forces, Synchronous machine, Simulation*

Abstract *The technique for the simulation of the dynamic behaviour of rotating machines presented in the paper is based on an equivalent circuit representation of the magnetic configuration. The circuit parameters are obtained by a preliminary automated sequence of magnetostatic FEM analyses and take into account the local magnetic saturations. The adopted solution technique is based on an invariant network topology approach: its application, presented for the operation analysis of a low-power synchronous generator, allows a great reduction of the calculation time in comparison with a commercial FEM code for the transient simulation.*

Introduction

For many years, the most commonly used tool in advanced design and study of electromagnetic devices has been represented by the electromagnetic FEM analysis (Kunze *et al.*, 1991; Nabeta *et al.*, 1996; Preston and Sturgess, 1993; Schmidt *et al.*, 2000, 2001).

More recent implementations of the FEM-based codes allow the transient simulation, taking into account the dependence of both the sources and the geometrical configuration on time. Nevertheless, the steep application of such codes does not allow a deep insight into the electromagnetic behaviour and generally results in high calculation times, even if a single configuration has to be analysed under various operative conditions. Getting worse, the performance assessment in consideration of parametric variations is time-consuming in proportion to the number of configurations to be examined.

Low-power synchronous generators emphasize such problems, due to the relevant "cross-coupling" effect between the d and q axes m.m.f.s caused by the high local saturation in the pole shoe zone.

The alternative approach, presented in this paper, is based on the representation of the synchronous machines by an equivalent magnetic circuit (Andriollo *et al.*, 2001), whose various elements accurately characterise the behaviour of different zones by suitable magnetic permeances (reluctances) and m.m.f.s. Such method, implemented in a code, allows the fast and accurate

Work financed by the Italian National Ministry of Education, University and Research (MIUR), Cofin 1999, Title: "Electromagnetic analysis, modelling and design optimisation of low-power synchronous generators".

COMPEL: The International Journal for Computation and Mathematics in Electrical and Electronic Engineering
Vol. 22 No. 4, 2003
pp. 953-968

0332-1649
DOI 10.1108/03321640310482922

calculation of the winding flux linkages, given the rotor position and the winding currents.

An effective procedure for the transient analysis was then obtained, integrating such code in a step-by-step procedure for the numerical integration of the voltage differential equations. Several integration techniques were considered, and their performances from the numerical viewpoint were investigated.

In the examples of application, the results obtained by the code based on the proposed technique are compared with the ones related to a commercial FEM code for the electromagnetic transient analysis (Ansoft Maxwell 2D Transient Code, v.8.0.22, 2001).

Determination of the flux linkages

To illustrate and test the method, a 2D typical configuration is considered (Figure 1(a)), related to a 2-poles 3-phase synchronous generator with 24 stator slots, with single-layer windings.

It exhibits all the local saturation phenomena, particularly relevant in the low power machines; in order to evidence the cogging effects due to the stator teeth, an open slot configuration was considered, even if it is not used in actual machines. Various circuit patterns were examined, related to different geometrical subdivisions; a good agreement with the results of the corresponding FEM analyses was obtained by the circuit representation of Figure 1(b), related to the partition of Figure 1(a) (Andriollo *et al.*, 2001).

The nodes s_i, c_i ($i = 0, \ldots, n_s - 1$ with $n_s = 24$ number of stator slots) and r_j ($j = 0, \ldots, n_r - 1$ with $n_r = 8$ divisions of the rotor surface) identify, respectively, stator teeth, stator yoke radial sections and rotor boundaries (configuration symmetry was deliberately ignored, to demonstrate the procedure applicability also to unsymmetrical structures).

Parameters of the magnetic circuit

The configuration is subdivided into different magnetic zones, the permeance of which (or reluctance) is represented alternatively as:

- a linear parameter, unaffected by the load condition, but generally dependent on the stator-rotor relative position, for the magnetic paths in air (air-gap and leakage);
- a flux-dependent parameter, for paths mainly developing inside ferromagnetic branches, and therefore approximately restricted in a time-independent geometrical structure, but affected by the magnetic saturation.

The air-gap permeances are distinguished in:

- "mutual" air-gap permeances ($\lambda_{i,j}$), related to the fluxes flowing between the ith stator tooth edge and the jth rotor boundary edge;

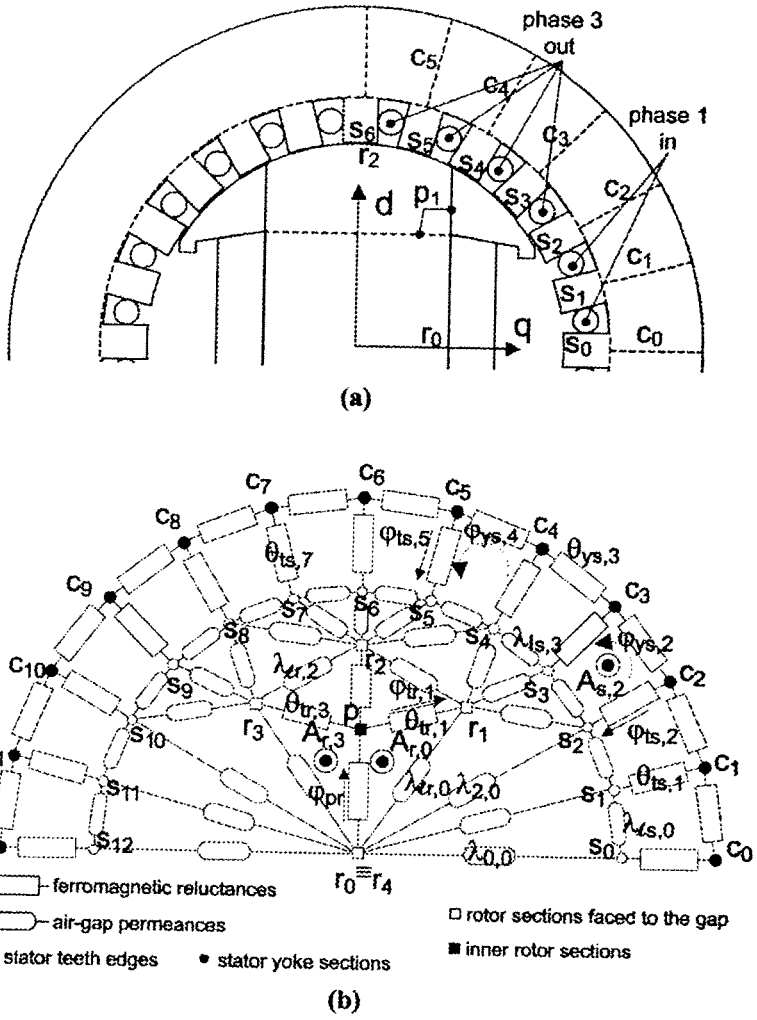

Figure 1.
Synchronous machine structure and model: (a) machine structure considered for the analysis (dashed lines: boundaries of the ferromagnetic branches); (b) equivalent magnetic network (only some representative elements are shown and labelled)

- air-gap leakage permeances ($\lambda_{es,i}$ and $\lambda_{er,j}$), associated to the fluxes between ith and $(i+1)$th stator teeth and between jth and $(j+1)$th rotor boundaries, respectively.

An automated sequence of FEM analyses allows to calculate the air-gap permeances. In order to perform these evaluations, an infinite magnetic permeability μ_{Fe} of the iron core must be provisionally assumed: the air-gap permeances are obtained as the ratio between the fluxes (flowing between the involved zone and the adjacent ferromagnetic surfaces) and the difference of the magnetic potential impressed by means of suitable probe sources. The interpolation of the results obtained by such analyses sequence allows to define the various permeances as functions of the rotor position α (Figure 2(a)).

According to such scheme, each stator tooth is ideally coupled with each rotor zone and vice versa for every position α (in practice, the related

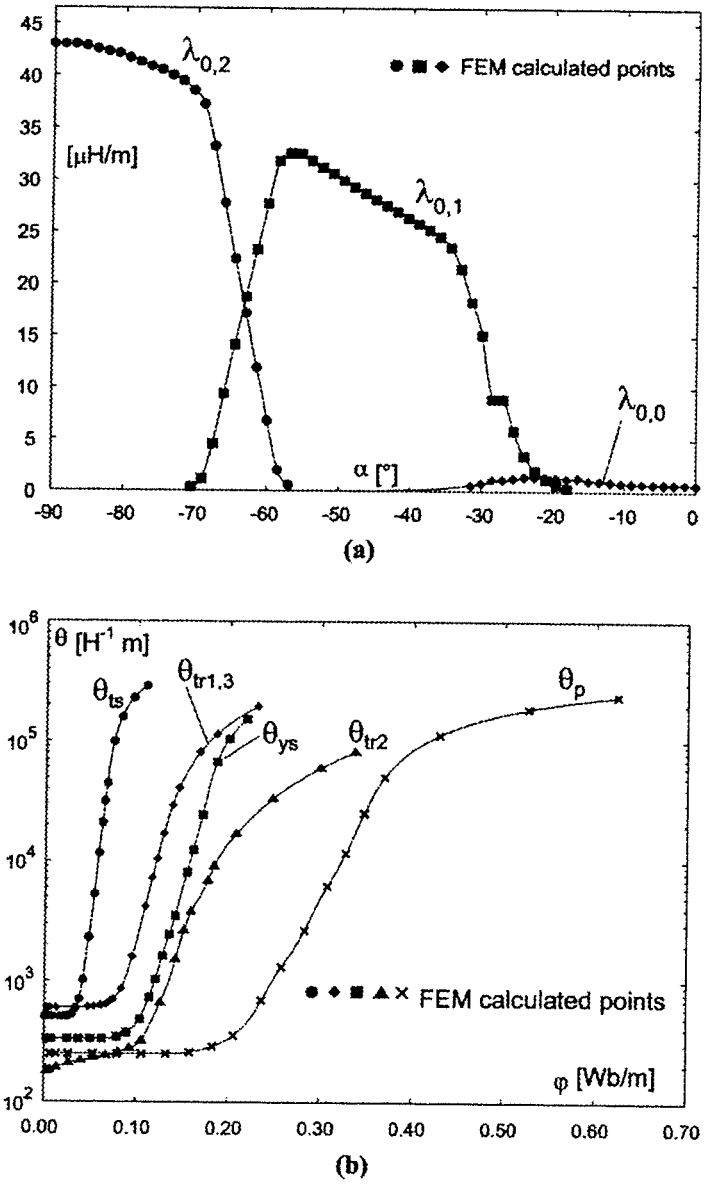

Figure 2.
(a) Air-gap permeances as functions of the rotor position α; (b) iron core reluctances as functions of the proper branch fluxes (θ_{ts}: stator teeth; θ_{ys}: stator yoke sections; $\theta_{tr1,3}$: polar shoe expansions; θ_p: polar bodies)

permeance function rapidly decays as the distance between the two zones increases). Hence, the network structure, albeit non-planar, is time-invariant, the dependence on α being assigned to the permeance values: this choice greatly simplifies the analysis, because no topological update is needed during rotation.

Also the iron core reluctances are evaluated via a suitable sequence of automated FEM analyses (Andriollo *et al.*, 2001):

- the flux φ in each considered branch is evaluated by a non-linear FEA, applying suited probe m.m.f. sources, taking into account the proper

non-linear $B(H)$ relationship for that ferromagnetic branch and assuming $\mu_{Fe} \rightarrow \infty$ in the rest of the iron core;

- the air-gap magnetic voltage drop (MVD) can be determined by evaluating the corresponding air-gap permeance, as previously explained;
- deducting the air-gap MVD contribution from the total MVD, the drop in the ferromagnetic branch and the corresponding reluctance θ is calculated;
- the previous steps are repeated for different values of the probe m.m.f. sources;
- the interpolation of $\{\theta,\varphi)$ values gives the non-linear function $\theta(\varphi)$ (Figure 2(b)).

Non-linear magnetic circuit solution algorithm

While some solvers were previously developed, just for the analysis of no-load conditions (Di Gerlando *et al.*, 1995), the following method described leads to direct and general formulations; its integration in an efficient code for transient analysis allows good performances from the point of view of both the accuracy and speed of calculation. The solution of the magnetic network is based on explicit recursive formulations of the magnetic potentials of the nodes s_i, c_i and subsequent expressions of the fluxes on iron core branches.

With reference to the circuit of Figure 1(b), let us introduce some further magnetic stator and rotor quantities:

$U_{s,i}$ – magnetic potential of the ith stator tooth head;

$\varphi_{ts,i}$ – flux flowing out the ith stator tooth;

$\varphi_{ys,i}$ – flux flowing through the stator yoke section between the ith and the $(i+1)$th teeth;

$A_{s,i}$ – ampere turns in the ith stator slot (between the ith and the $(i+1)$th teeth);

$U_{r,j}$ – magnetic potential of the jth rotor zone surface;

$\varphi_{tr,j}$ – flux flowing out through the jth rotor zone;

φ_{pr} – flux flowing through the rotor pole;

$A_{r,j}$ – ampere-turns related to rotor lap embraced by the jth and the $(j+1)$th zone.

Calculation of the scalar magnetic potentials

Stator. With reference to the generic lap of the ith stator slot, the following n_s recursive equations hold ($i = 0, 1, \ldots, n_s - 1$; $\overline{i+1}$ is the remainder of the division of $i+1$ by n_s, so that when $i = n_s - 1$, $\overline{i+1} = 0$; similarly, for $i = 0$, $\overline{i-1} = n_s - 1$):

$$U_{s,\overline{i+1}} - U_{s,i} = A^*_{s,i}, \tag{1}$$

with

$$A^*_{s,i} = A_{s,i} - \theta_{ts,\overline{i+1}}\varphi_{ts,\overline{i+1}} - \theta_{ys,i}\varphi_{ys,i} + \theta_{ts,i}\varphi_{ts,i} \tag{2}$$

The terms $A^*_{s,i}$ represent the slot ampere-turns lessened by the magnetic potential drops due to teeth and yoke reluctances. The fluxes conservation implies that:

$$\varphi_{ts,i} = \varphi_{ys,\overline{i-1}} - \varphi_{ys,i} \tag{3}$$

To solve the set of equation (1), the further equation is introduced:

$$\sum_{i=0}^{n_s-1} \lambda_{s,i} U_{s,i} = 0 \tag{4}$$

where

$$\lambda_{s,i} = \sum_{j=0}^{n_r-1} \lambda_{i,j}$$

is the ith stator tooth gap permeance; the following relation is obtained:

$$U_{s,0} = -\frac{\sum_{i=1}^{n_s-1} \lambda_{s,i} F^*_{s,i-1}}{\sum_{i=0}^{n_s-1} \lambda_{s,i}} = -\frac{\sum_{i=1}^{n_s-1} \lambda_{s,i} F^*_{s,i-1}}{\Lambda_{s,r}} \tag{5}$$

with

$$F^*_{s,i} = \sum_{h=0}^{i} A^*_{s,h}$$

and

$$\Lambda_{s,r} = \sum_{i=0}^{n_s-1} \lambda_{s,i} = \sum_{i=0}^{n_s-1} \sum_{j=0}^{n_r-1} \lambda_{i,j},$$

being $\Lambda_{s,r}$ the global permeance between the stator and rotor.

By means of equation (5), the other potentials $U_{s,i}$ are determined by the recursive relation (1).

Rotor. With reference to Figure 1(b), a sequence of rotor magnetic laps analogous to the stator ones can be recognised, and a set of $n_r - 1$ recursive equations like (1) could be therefore obtained. Taking advantage of the

geometrical and magnetic symmetry, the problem is simplified, since only $n_r/2$ equations are required, corresponding to contiguous rotor laps embracing a 180° arc (it results $U_{r,j+nr/2} = -U_{r,j}$). Defining the quantities related to the rotor ampere-turns:

$$\begin{aligned} A^*_{r,0} &= A_{r,0} + \theta_{tr,1}\varphi_{tr,1} + \theta_p\varphi_{pr} \\ A^*_{r,1} &= A_{r,1} + \theta_{tr,2}\varphi_{tr,2} - \theta_{tr,1}\varphi_{tr,1} \\ A^*_{r,2} &= A_{r,2} + \theta_{tr,3}\varphi_{tr,3} - \theta_{tr,2}\varphi_{tr,2} \\ A^*_{r,3} &= A_{r,3} - \theta_p\varphi_{pr} - \theta_{tr,3}\varphi_{tr,3} \end{aligned} \tag{6}$$

the following equations are obtained:

$$\begin{aligned} U_{r,0} &= F^*_{r,3}/2 = \frac{\left(A^*_{r,0} + A^*_{r,1} + A^*_{r,2} + A^*_{r,3}\right)}{2} \\ U_{r,1} &= U_{r,0} - F^*_{r,0} \\ U_{r,2} &= U_{r,0} - F^*_{r,1} \\ U_{r,3} &= U_{r,0} - F^*_{r,2} \end{aligned} \tag{7}$$

with

$$F^*_{r,j} = \sum_{k=0}^{i} A^*_{r,k}.$$

Calculation of fluxes

Stator. Once the stator and rotor potentials are defined, the flux delivered by the generic ith stator tooth is given by:

$$\varphi_{ts,i} = -\lambda_{ts,\overline{i-1}}U_{s,\overline{i-1}} + \lambda^*_{s,i}U_{s,i} - \lambda_{ts,i}U_{s,\overline{i+1}} - \sum_{j=0}^{n_r-1}\lambda_{ij}U_{r,j} \tag{8}$$

with $\lambda^*_{s,i} = \lambda_{s,i} + \lambda_{ts,i} + \lambda_{ts,\overline{i-1}}$ the ith tooth total gap permeance.

Rearranging equation (3), the stator yoke fluxes can be explicited as in the following:

$$\begin{aligned}
\varphi_{ys,1} &= -\psi_{s,1} + \varphi_{ys,0} \\
\varphi_{ys,2} &= -\psi_{s,2} + \varphi_{ys,0} \\
&\vdots \\
\varphi_{ys,n_s-1} &= -\psi_{s,n_s-1} + \varphi_{ys,0}
\end{aligned} \tag{9}$$

with

$$\psi_{s,i} = \sum_{h=1}^{i} \varphi_{ts,h}$$

Since the net m.m.f. acting inside the stator yoke is null, the sum of the MVDs along the yoke must be zero, i.e.:

$$\sum_{i=0}^{n_s-1} \theta_{ys,i}\varphi_{ys,i} = 0 \tag{10}$$

Combining equations (9) and (10), $\varphi_{ys,0}$ can be expressed as:

$$\varphi_{ys,0} = \frac{\sum_{i=1}^{n_s-1} \theta_{ys,i}\psi_{s,i}}{\sum_{i=1}^{n_s-1} \theta_{ys,i}} \tag{11}$$

and so all the other stator yoke fluxes can be determined.

Rotor. The flux in the jth rotor zone can be expressed as a function of the magnetic potentials in the form:

$$\varphi_{tr,j} = -\lambda_{tr,\overline{j-1}}U_{r,\overline{j-1}} + \lambda^*_{r,j}U_{r,j} - \lambda_{tr,j}U_{r,j+1} - \sum_{i=0}^{n_s-1} \lambda_{ij}U_{s,i} \tag{12}$$

with $\lambda^*_{r,j} = \lambda_{r,j} + \lambda_{tr,j} + \lambda_{tr,\overline{j-1}}$ the jth zone gap permeance.

The rotor pole flux φ_{pr} is then obtained by:

$$\varphi_{pr} = \varphi_{tr,1} + \varphi_{tr,2} + \varphi_{tr,3} \tag{13}$$

The previous equations define a non-linear system, requiring an iterative procedure to be solved. In such application, a fixed-point technique is adopted: let $\underline{X}_{(n)}$ be the set of values of the magnetic circuit quantities (ampere-turns, magnetic potentials, fluxes) evaluated at the nth step. Entering such values in

the previous equations, a preliminary updated set $\underline{X}^{u}_{(n+1)}$ is obtained; the new solution vector $\underline{X}_{(n+1)}$ is then determined as:

$$\underline{X}_{(n+1)} = \beta \underline{X}^{u}_{(n+1)} + (1-\beta)\underline{X}^{u}_{(n+1)}. \tag{14}$$

A suited choice of the relaxation factor $\beta < 1$ is essential to prevent the numerical instability, limiting at the same time the number of iterations: the higher the saturation, the lower is the instability threshold value of β. The convergence estimation is based on the calculation of the flux variation $\Delta\varphi_{(n)}$ from the $(n-1)$th to the nth iteration (sub-subscripts $(n-1)$ and (n)):

$$\Delta\varphi_{(n)} = \frac{\sum_{i=0}^{n_s-1}\left(\underset{(n)}{\varphi_{ts,i}} - \underset{(n-1)}{\varphi_{ts,i}}\right)^2 + \sum_{j=0}^{n_r-1}\left(\underset{(n)}{\varphi_{tr,j}} - \underset{(n-1)}{\varphi_{tr,j}}\right)^2}{\sum_{i=0}^{n_s-1}\underset{(n)}{\varphi^2_{ts,i}} + \sum_{j=0}^{n_r-1}\underset{(n)}{\varphi^2_{tr,j}}} \tag{15}$$

The iterations are continued until the number n exceeds a maximum n_{max} or $\Delta\varphi_{(n)}$ goes below a threshold value ε_{φ}.

The process is outlined by the flow diagram of Figure 3.

Determination of the flux linkages

The stator winding flux linkages ψ_1, ψ_2, ψ_3 are determined by multiplying the fluxes $\varphi_{ts,i}$ with the linkage coefficients $\{w_{p,0}, \ldots, w_{p,n_s-1}\}$ of the pth phase winding, according to the following formulations:

$$\psi_p = \sum_{i=0}^{n_s-1} w_{p,i}\varphi_{ts,i} \quad \text{with } p = 1,2,3$$

$$w_{p,i} = w'_{p,i-1} - \frac{1}{n_s}\sum_{i=0}^{n_s-1} w'_{p,i} \tag{16}$$

$$w'_{p,0} = 0, \quad w'_{p,i+1} = w'_{p,i} + \gamma_{p,i} \text{ with } i = 0, \ldots, n_s - 2$$

The pth phase connection coefficients $\gamma_{p,i}$ are given by the number of conductors in the ith slot with a leading + if current flows towards the reader, − if it flows in the opposite direction, 0 if pth phase has no conductor in the slot.

For a symmetrical 3-phase winding, once the phase 1 linkage coefficients are determined, the corresponding ones for phases 2 and 3 are simply

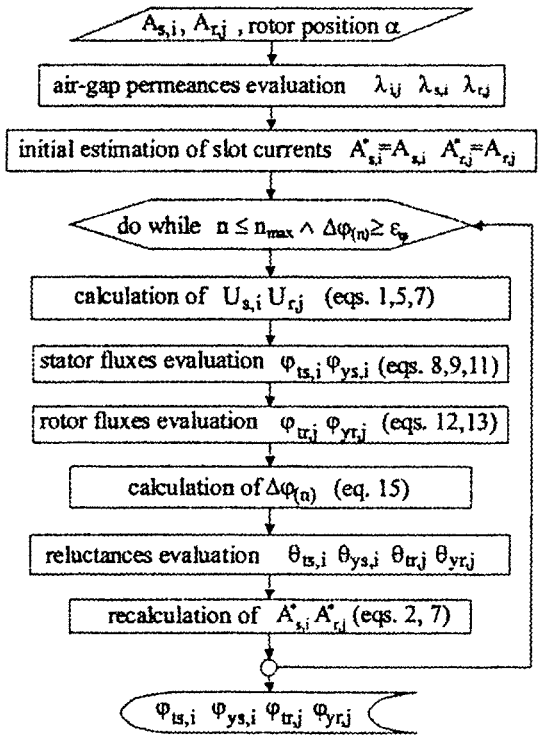

Figure 3.
Outline of the procedure for the fluxes calculation

obtained by shifting the coefficients to the left of $n_s/3$ and $2n_s/3$ positions, respectively.

Analogous expressions can be defined for the rotor windings. More directly, the flux linkage of the N_e turns excitation winding is given by:

$$\psi_e = -N_e(\varphi_{tr,1} + \varphi_{tr,2} + \varphi_{tr,3}). \tag{17}$$

Procedure for the transient analysis

With reference to Figure 4, let $\underline{v} = \{v_1 - v_0, v_2 - v_0, v_3 - v_0, v_e\}$, $\underline{i} = \{i_1, i_2, i_3, i_e\}$, $\underline{\psi} = \{\psi_1, \psi_2, \psi_3, \psi_e\}$ be the voltage, current and flux vectors, respectively (*e*-subscripted quantities refer to the excitation winding, the other elements to the armature phases). Consider the voltage equations as written according to the active bipole representation and express them in the matrix form:

$$\begin{aligned} \underline{v} &= \frac{d\underline{\psi}}{dt} - \underline{R}_w \cdot \underline{i} \\ v_p - v_0 &= R_l i_p + L_l \frac{di_p}{dt} \quad (p = 1,2,3), \quad v_e = -V_e \end{aligned} \tag{18}$$

with $\underline{R}_w$ diagonal matrix related to the winding resistances $\{R_a, R_a, R_a, R_e\}$ and V_e field supply constant voltage.

The wye midpoint voltage v_0 can be determined according to the characteristics of the neutral connection: if such connection, as in most cases, is absent (i.e. $i_1 + i_2 + i_3 = 0$), the sum of the armature winding equations gives:

$$v_0 = p\left(\frac{\psi_1 + \psi_2 + \psi_3}{3}\right) = p\psi_0 \tag{19}$$

with ψ_0 the homopolar component of the flux.

According to equation (19), equation (18) can be rearranged as:

$$\begin{aligned} v_p &= R_l i_p + L_l \frac{di_p}{dt} = -\frac{d}{dt}(\psi_p - \psi_0) - R_a i_p \quad p = 1,2,3 \\ v_e &= -V_e = -\frac{d\psi_e}{dt} - R_e i_e \end{aligned} \tag{20}$$

Defining the equivalent global flux linkages $\phi_p = \psi_p - \psi_0 + L_l i_p$ and including the armature winding resistances in the resistance diagonal matrix $\underline{R}$ with non-null elements $\{R_a + R_l,\ R_a + R_l,\ R_a + R_l,\ R_e\}$, equation (20) rearranged as:

$$\underline{u} = \frac{d\underline{\phi}}{dt} + \underline{R} \cdot \underline{i} \quad \text{with} \quad \underline{u} = \{0,0,0,V_e\} \quad \text{and} \quad \underline{\phi} = \{\phi_1, \phi_2, \phi_3, \phi_e\} \tag{21}$$

Referring the subscripts $(k,\ k+1)$ to $t_k,\ t_{k+1}$, respectively, and posing $\alpha_{k+1} - \alpha_k = \omega \cdot \Delta t$, with rotational speed ω and Δt = constant the integration of equation (21) from t_k to $t_{k+1} = t_k + \Delta t$ by the trapezoidal rule yields:

$$\frac{\underline{u}_{k+1} + \underline{u}_k}{2}\Delta t = \underline{R} \cdot \frac{\underline{i}_{k+1} + \underline{i}_k}{2}\Delta t + (\underline{\phi}_{k+1} - \underline{\phi}_k) \tag{22}$$

Evidencing the occurring $(k+1)$th state quantities $\underline{i}_{k+1},\ \underline{\phi}_{k+1}$, it results:

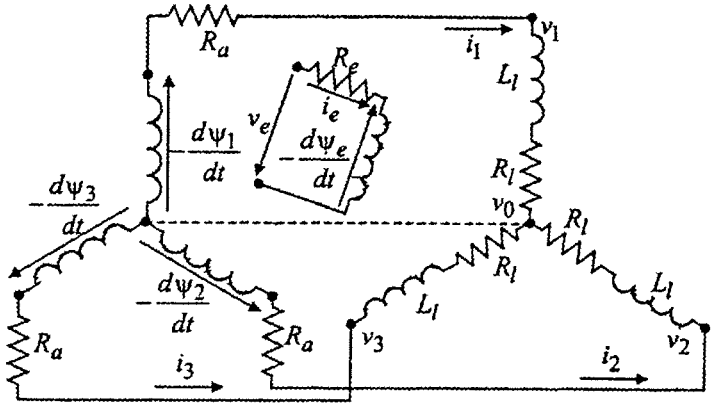

Figure 4.
Circuit representation of the armature and excitation windings (R_a: armature phase resistance; R_l, L_l: load resistance and inductance; R_e: excitation winding resistance)

$$\underline{i}_{k+1} + \frac{2}{\Delta t}\underline{\underline{R}}^{-1} \cdot \underline{\phi}_{k+1} = \underline{\underline{R}}^{-1} \cdot \frac{\underline{u}_{k+1} + \underline{u}_k}{2} - \underline{i}_k + \frac{2}{\Delta t}\underline{\underline{R}}^{-1} \cdot \underline{\phi}_k \tag{23}$$

where all the right-side quantities are known, as soon as the previous kth state is determined. Due to the non-linear dependence of $\underline{\phi}_{k+1}$ on $\underline{i}_{k+1}$, equation (23) has to be solved via an iterative algorithm, according to the following points (where (q), $(q-1)$ superscripts denote the values related to the current qth iteration and to the previous one, respectively):

- the flux $\underline{\phi}_{k+1}^{(q)}$ can be expressed by its Taylor series expansion arrested to the first-order term, starting from the previous estimated values $\{\underline{\phi}_{k+1}^{(q-1)}, \underline{i}_{k+1}^{(q-1)}\}$:

$$\underline{\phi}_{k+1}^{(q)} = \underline{\phi}_{k+1}^{(q-1)} + \left.\frac{\partial \underline{\underline{\phi}}}{\partial \underline{i}}\right|_{k+1}^{(q-1)} \cdot \left(\underline{i}_{k+1}^{(q)} - \underline{i}_{k+1}^{(q-1)}\right) \tag{24}$$

- substituting equation (24) in equation (23) and collecting $\underline{i}_{k+1}^{(q)}$ yields:

$$\left(\underline{\underline{I}} + \frac{2}{\Delta t}\underline{\underline{R}}^{-1} \cdot \left.\frac{\partial \underline{\underline{\phi}}}{\partial \underline{i}}\right|_{k+1}^{(q-1)}\right)\underline{i}_{k+1}^{(q)} = -\frac{2}{\Delta t}\underline{\underline{R}}^{-1} \cdot \left(\underline{\phi}_{k+1}^{(q-1)} - \left.\frac{\partial \underline{\underline{\phi}}}{\partial \underline{i}}\right|_{k+1}^{(q-1)} \underline{i}_{k+1}^{(q-1)}\right) \tag{25}$$

$$+ \underline{\underline{R}}^{-1} \cdot (\underline{u}_{k+1} + \underline{u}_k) - \underline{i}_k + \frac{2}{\Delta t}\underline{\underline{R}}^{-1} \cdot \underline{\phi}_k$$

with $\underline{\underline{I}}$ 4×4 identity matrix; finally $\underline{i}_{k+1}^{(q)}$ is given by:

$$\underline{i}_{k+1}^{(q)} = \left(\underline{\underline{R}}\frac{\Delta t}{2} + \left.\frac{\partial \underline{\underline{\phi}}}{\partial \underline{i}}\right|_{k+1}^{(q-1)}\right)^{-1} \cdot \left(\underline{\phi}_k - \underline{\phi}_{k+1}^{(q-1)} + \left.\frac{\partial \underline{\underline{\phi}}}{\partial \underline{i}}\right|_{k+1}^{(q-1)} \cdot \underline{i}_{k+1}^{(q-1)}\right. \tag{26}$$

$$\left. + (\underline{u}_{k+1} + \underline{u}_{k+1} - \underline{\underline{R}} \cdot \underline{i}_k)\frac{\Delta t}{2}\right);$$

- the quantities

$$\underline{\phi}_{k+1}^{(q)}, \left.\frac{\partial \underline{\underline{\phi}}}{\partial \underline{i}}\right|_{k+1}^{(q)}$$

can be quickly determined via the method of solution of the magnetic network described earlier;

- as starting values ($q = 0$), the following ones are assumed (α value has to be updated from α_k to α_{k+1}):

$$\underline{i}_{k+1}^{(0)} = \underline{i}_k$$

$$\underline{\phi}_{k+1}^{(0)} = \underline{\phi}\left(\underline{i}_{k+1}^{(0)}, \alpha_{k+1}\right) \quad \left.\frac{\partial \underline{\phi}}{\partial \underline{i}}\right|_{k+1}^{(0)} = \frac{\partial \underline{\phi}}{\partial \underline{i}}\left(\underline{i}_{k+1}^{(0)}, \alpha_{k+1}\right) \tag{27}$$

indicating with $\underline{N}$ the diagonal matrix containing the number of the winding turns and with $\overline{\varepsilon_i}$ a predefined threshold value, the iteration is stopped when the relative value of the ampere-turns variation, $\Delta i_{(q)}$ verifies the following condition:

$$\Delta i_{(q)} = \frac{\left\| \underline{N} \cdot \underline{i}_{k+1}^{(q)} - \underline{N} \cdot \underline{i}_{k+1}^{(q-1)} \right\|}{\left\| \underline{N} \cdot \underline{i}_{k+1}^{(q)} \right\|} < \varepsilon_i. \tag{28}$$

Examples of application

The described technique was applied to the purely hypothetical configuration sketched in Figure 1(a), in order to compare the results with the ones obtained by a commercial FEM code for the electromagnetic transient analysis (Ansoft Maxwell 2D Transient Code, v.8.0.22, 2001). A time step $\Delta t = 50\,\mu$s (angular step: $\omega \Delta t\, 180°/\pi = 0.9°$) was adopted in the proposed procedure to achieve an adequate angular resolution, while $\Delta t = 138.9\,\mu$s (angular step: 2.5°) in the FEM transient analysis. Mechanical transient was neglected, assuming a constant rotation speed $\omega = 314.16\,\text{s}^{-1}$ (3,000 rpm).

No-load excitation current build-up

As a first case, the excitation current build-up at no load was considered, starting from null initial value and applying a constant voltage $V_e = 100\,\text{V}$ to the field winding ($N_e = 1,260$ turns, $R_e = 20\,\Omega$). To reach a nearly complete steady state running, more than 8 s are required. Figures 5 and 6 show the current i_e and flux linkage ψ_e of the excitation winding, respectively, as functions of time, comparing the results of the proposed procedure and FEM transient analysis. The cogging effect on the excitation current is evidenced in Figure 5(b). The relative difference is about 3 per cent for the current values, and ≈ 1.3 per cent with reference to the fluxes.

Simulation of load insertion

A sudden load insertion ($R_a + R_l = 3.2\,\Omega$) at $t = 0\,\text{s}$ was simulated maintaining $V_e = 100\,\text{V}$ and assuming initial current values $\{i_1, i_2, i_3, i_e\} = \{0, 0, 0, 5\,\text{A}\}$. The currents and the flux linkages of the armature windings in the early instants of the transient are compared with the FEM results in Figure 7, showing a good agreement.

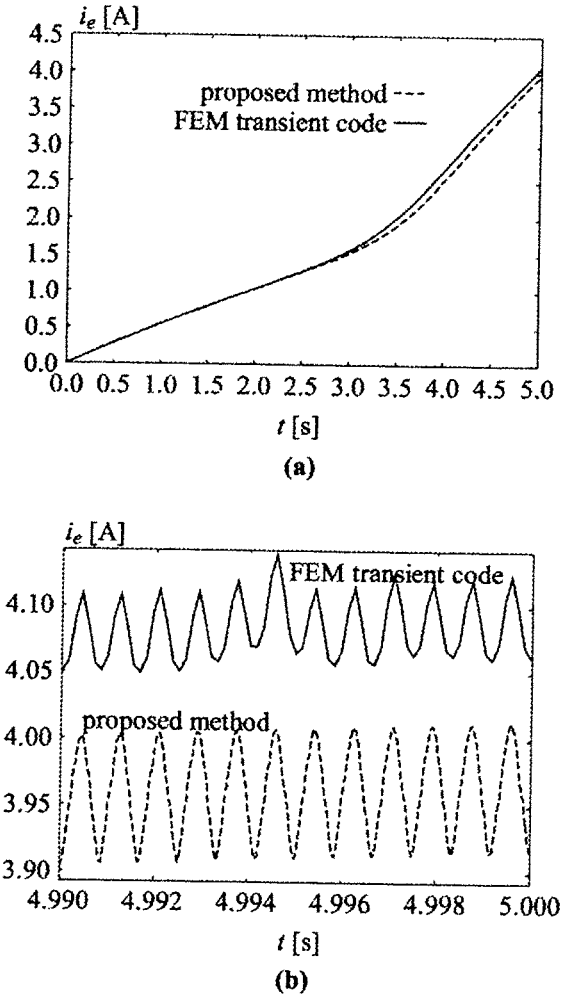

Figure 5.
No-load field current i_e: (a) during the entire simulation (with ripple smoothing for sake of clearness); (b) focused for 10 ms period to display the cogging effect

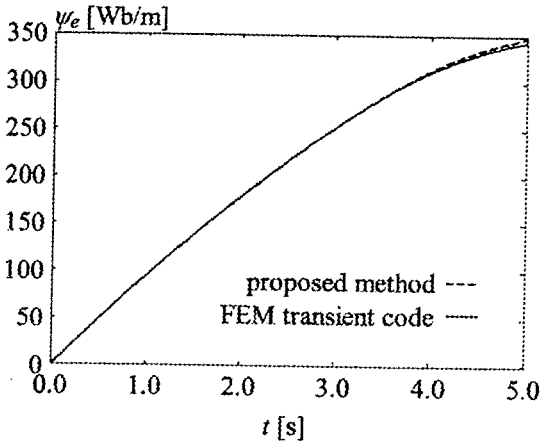

Figure 6.
Build-up of the excitation flux ψ_e at no-load

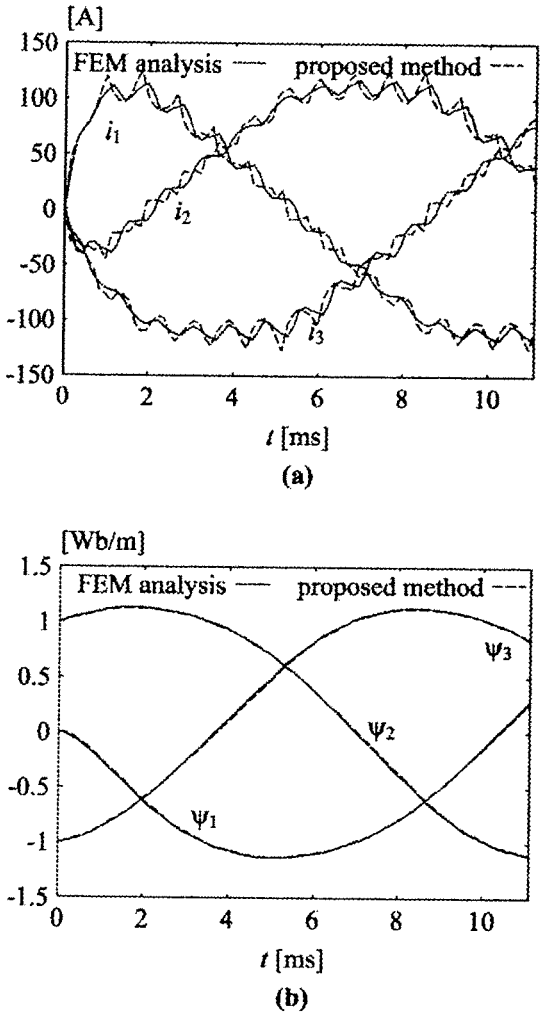

Figure 7.
(a) Armature currents and (b) flux linkages after a resistive load insertion

It is worth to remark that the calculation time with the FEM code is at least one order of magnitude higher than that of the proposed method, the same time resolution being maintained.

Conclusions

A method for the electromagnetic transient analysis of synchronous machines, based on the solution of an equivalent magnetic circuit, was described. Such method could be extended to a wider class of electromechanical devices with minor modifications of the algorithmic structure.

The examples of application of a code, based on such method, show a good agreement with the results of a commercial FEM code, allowing on the other hand a great reduction in the calculation time.

References

Andriollo, M., Di Gerlando, A. and Porzio, D. (2001), "A design oriented magnetic circuit model of low-power synchronous generators", *Proceedings of the 4th International Symposium on Advanced Electromechanical Motion Systems – Electromotion '01*, 19-20 June 2001, Bologna, Italy, pp. 535-40.

Ansoft Maxwell 2D Transient Code v.8.0.22 (2001).

Di Gerlando, A., Perini, R. and Vistoli, I. (1995), "A field-circuit approach to the design oriented evaluation of the no-load voltage harmonics of salient pole synchronous generators", *Conference Electric Machines and Drives 95*, Durham, UK, pp. 390-4.

Kunze, W., Kuß, H. and Bölter, F-Tth. (1991), "Application of numerical field calculation to selected problems of electrical machines", *Conference SM100*, Zurich, CH, pp. 1193-8.

Nabeta, S.I., Foggia, A., Coulomb, J.L. and Reyne, G. (1996), "Finite element simulations of unbalanced faults in a synchronous machine", *IEEE Transactions on Magnetics*, Part 1, Vol. 32 No. 3, pp. 1561-4.

Preston, T.W. and Sturgess, J.P. (1993), "Implementation of the finite-element method into machine design procedures", *6th International Conference on Electrical Machines and Drives*, pp. 312-17.

Schmidt, E., Grabner, C. and Traxler-Samek, G. (2000), "Reactance calculation of a 500 MVA hydro-generator using a finite element analysis with superelements ", *Electric Machines and Drives Conference*, pp. 838-44

Schmidt, E., Grabner, C. and Traxler-Samek, G. (2001), "Determination of reactances of large hydro-generators using finite elements and domain decomposition", *Canadian Conference on Electrical and Computer Engineering*, Vol. 2, pp. 811-17.

Further reading

Ostovich, V. (1989), *Dynamics of Saturated Machines*, Springer-Verlag, New York.

Sturgess, J.P. and Preston, T.W. (1993), "Damper cage design using the finite-element method", *Conference on Electrical Machines and Drives*, Oxford, UK, pp. 457-62.